

NMDA Receptor Expression by Retinal Ganglion Cells Is Not Required for Retinofugal Map Formation Nor Eye-specific Segregation In The Mouse

<https://doi.org/10.1523/ENEURO.0115-20.2021>

Cite as: eNeuro 2021; 10.1523/ENEURO.0115-20.2021

Received: 20 March 2020

Revised: 19 May 2021

Accepted: 21 May 2021

This Early Release article has been peer-reviewed and accepted, but has not been through the composition and copyediting processes. The final version may differ slightly in style or formatting and will contain links to any extended data.

Alerts: Sign up at www.eneuro.org/alerts to receive customized email alerts when the fully formatted version of this article is published.

Copyright © 2021 Johnson et al.

This is an open-access article distributed under the terms of the Creative Commons Attribution 4.0 International license, which permits unrestricted use, distribution and reproduction in any medium provided that the original work is properly attributed.

1 **Title:** NMDA Receptor Expression by Retinal Ganglion Cells Is Not Required for Retinofugal
2 Map Formation Nor Eye-specific Segregation In The Mouse

3
4 **Abbreviated Title:** Role of RGC NMDARs in retinofugal organization in mice

5
6 Author Names and Affiliations: Kristy O. Johnson^{1,2}, Nathan A. Smith^{1,3,4}, Evan Z. Goldstein¹,
7 Vittorio Gallo^{1,2,3,4}, and Jason Triplett^{1,2,3,4}

8
9 ¹Center for Neuroscience Research, Children's National Research Institute, Washington, DC
10 20010

11 ²Institute for Biomedical Sciences, The George Washington University School of Medicine &
12 Health Sciences, Washington, DC 20052

13 ³Department of Pediatrics, The George Washington University School of Medicine & Health
14 Sciences, Washington, DC 20052

15 ⁴ Department of Pharmacology & Physiology, The George Washington University School of
16 Medicine & Health Sciences, Washington, DC 20052

17
18 Author Contributions: K.O.J Designed research, Performed research, Analyzed data, and Wrote
19 the paper; N.A.S Designed and Performed research; E.Z.G Designed and Performed research,
20 V.G Designed research; J.W.T Designed research and Wrote the paper

21
22 *Corresponding Author

23 Jason Triplett, PhD
24 111 Michigan Ave, NW M7632
25 Washington, DC 20010
26 (202)476-3985

27 jtriplett@childrensnational.org

28

29 Number of Figures: 7

30 Number of Tables: 0

31 Number of Multimedia: 0

32 Number of words for Abstract: 229

33 Number of words for Significance Statement: 86

34 Number of words for Introduction: 662

35 Number of words for Discussion: 1548

36

37 Acknowledgments: We thank members of the Triplett and Corbin labs for helpful discussions.

38 Microscopic imaging and analysis were carried out at the Children's National Research Institute

39 (CNRI) Cell and Tissue Microscopy Core supported by CNRI and DC-IDDRC grant

40 U54HD090257 by the National Institute of Child Health and Human Development.

41 Conflict of Interest: Authors report no conflict of interest.

42

43 Funding Sources: NIH R01 EY02567 (J.W.T.), NIH K01 NS110981 (N.A.S.), NIH U54

44 HD090257 District of Columbia Intellectual and Developmental Disabilities Research Center

45 program (V.G.), NIH R37 NS109478 (V.G.), NIH F32 NS106723 (E.G.)

46

47

48

49

50

51

52

53 **Abstract**

54 Retinal ganglion cells (RGCs) project topographically to the superior colliculus (SC) and dorsal
55 lateral geniculate nucleus (dLGN). Spontaneous activity plays a critical role in retinotopic
56 mapping in both regions; however, the molecular mechanisms underlying activity-dependent
57 refinement remain unclear. Previous pharmacologic studies implicate NMDA receptors
58 (NMDARs) in the establishment of retinotopy. In other brain regions, NMDARs are expressed on
59 both the pre- and post-synaptic side of the synapse, and recent work suggests that pre-synaptic
60 and post-synaptic NMDARs play distinct roles in retinotectal developmental dynamics. To
61 directly test the role of NMDARs expressed by RGCs in retinofugal map formation, we took a
62 conditional genetic knockout approach to delete the obligate GluN1 subunit of NMDARs in
63 RGCs. Here, we demonstrate reduced GluN1 expression in the retina of Chrnb3-
64 Cre;GluN1^{flox/flox} (pre-cKO) mice without altered expression in the SC. Anatomical tracing
65 experiments revealed no **significant** changes in termination zone size in the SC and dLGN of
66 pre-cKO mice, suggesting NMDAR function in RGCs is not **an absolute requirement** for
67 topographic refinement. Further, we observed no change in the eye-specific organization of
68 retinal inputs to the SC nor dLGN. To verify that NMDA induces activity in RGC terminals, we
69 restricted GCaMP5 expression to RGCs and confirmed induction of calcium transients in RGC
70 terminals. Together, these findings demonstrate that NMDARs expressed by RGCs are not
71 required for retinofugal **topographic** map formation nor eye-specific segregation in the mouse.

72

73 **Significance Statement**

74 Topographic organization of retinal inputs in the brain is **thought to be** critical for the efficient
75 relay of spatial information in the visual scene. Previous studies suggest NMDARs play a crucial
76 role in establishing topography in the superior colliculus; however, these studies could not
77 distinguish between potential pre- or post-synaptic roles. Here, we show NMDAR function in
78 retinal ganglion cells (RGCs) is not required for the establishment of topography. Further, we
79 find RGC NMDARs are not required to establish or maintain eye-specific laminae in
80 retinorecipient regions.

81

82 Introduction

83 Retinal ganglion cells (RGCs) project to two **main** image forming regions, the superior
84 colliculus (SC) and the dorsal lateral geniculate nucleus (dLGN), where their axon terminals are
85 organized topographically. The establishment of topography occurs in a protracted process
86 during the first week of postnatal life in the mouse (Johnson & Triplett, 2021). Initially, diffuse
87 terminations are refined to topographically appropriate locations in a manner dependent on a
88 combination of molecular cues (Feldheim & O'Leary, 2010), axon-axon competition (Triplett et
89 al., 2011), and neuronal activity (McLaughlin et al., 2003; Pfeifferberger et al., 2006).

90 The activity driving retinofugal projection refinement is spontaneous, consisting of highly
91 correlated bursts of action potentials, termed retinal waves, that propagate across the retina
92 (Meister et al., 1991; Wong et al., 1993) and are transferred to downstream areas (Ackman et
93 al., 2012). Retinal waves progress through three stages based on their mode of propagation,
94 mediated first by gap junctions, then acetylcholine, and finally glutamate. Disruption of
95 cholinergic waves perturbs retinotopic map formation in the SC and dLGN (McLaughlin et al.,
96 2003; Chandrasekaran et al., 2007; Cang et al., 2008; Xu et al., 2015). While it is clear the
97 normal pattern of retinal waves is critical for topographic map formation in the SC and dLGN,
98 the molecular mechanisms by which activity mediates these processes remain unclear.

99 *N*-methyl-*D*-aspartate receptors (NMDARs) are ionotropic glutamate receptors widely
100 expressed throughout the brain and play a critical role in activity-dependent synaptic
101 strengthening (Nicoll & Malenka, 1999). Previous studies suggest a critical role for NMDARs in
102 the establishment of retinocollicular connectivity. Indeed, pharmacological blockade showed a
103 disruption in retinocollicular map organization when applied locally to the SC (Simon et al.,
104 1992) or tectum (Cline & Constantine-Paton, 1989). Further, the receptive field size of SC
105 neurons was increased upon chronic blockade, and lesion-induced plasticity was disrupted
106 (Huang & Pallas, 2001). Intriguingly, NMDAR blockade resulted in dramatic changes to retinal
107 arborization dynamics (Rajan et al., 1999; Ruthazer et al., 2003; Munz et al., 2014), suggesting

108 a potential role for NMDARs localized to RGC terminals. However, pharmacologic studies of
 109 retinotopy could not elucidate the neuronal populations in which NMDAR activity was required.

110 While best studied for their function at the post-synaptic side of the synapse,
 111 accumulating evidence suggests that NMDARs may also be expressed pre-synaptically in many
 112 brain regions (Pittaluga & Raiteri, 1990; Aoki et al., 1994; and Paoletti et al., 2013; Bouvier et
 113 al., 2015; Bouvier et al., 2018), including visual cortical circuits where they mediate spike-timing-
 114 dependent plasticity of connections between neurons in layer 4 (L4) and L2/3 (Corlew et al.,
 115 2007; Bouvier et al., 2018). Previous studies suggest that developing RGCs express NMDARs
 116 raising the possibility they could be localized pre-synaptically in retinorecipient regions (Massey
 117 & Miller, 1990; Mittman et al., 1990; Watanabe et al., 1994). Indeed, recent work demonstrated
 118 that pre- and post-synaptic NMDARs have distinct but complementary roles in developmental
 119 plasticity in the retinotectal system (Kesner et al., 2020). However, whether NMDARs expressed
 120 by RGCs are required for topographic refinement remains unclear.

121 To address this, we took a conditional genetic approach to delete the obligate GluN1
 122 subunit of NMDARs in RGCs without altering its expression in retinorecipient regions, allowing
 123 us to determine the potential role of pre-synaptic NMDARs in retinocollicular and
 124 retinogeniculate circuit formation. We confirmed a reduction of GluN1 expression in the retina of
 125 *Chrn3-Cre;GluN1^{flox/flox}* (pre-cKO) mice by *in situ* hybridization and quantitative PCR.
 126 Surprisingly, neither the topographic refinement nor the eye-specific segregation of retinal inputs
 127 in the SC and dLGN were altered in pre-cKO mice, suggesting a minimal role for NMDAR
 128 function in RGCs in these processes. To probe whether NMDARs might be activated pre-
 129 synaptically, we prepared slices of the SC from mice expressing a genetically-encoded
 130 GCaMP5 restricted primarily to RGCs. Indeed, administration of NMDA induced modest Ca^{2+}
 131 transients, suggesting that NMDARs may be localized pre-synaptically in the mouse SC.
 132 Together, these data suggest a limited role for NMDARs expressed by RGCs in the
 133 development and maintenance of ordered projections to image-forming retinorecipient regions.

134 **Materials and Methods**

135 *Mice*

136 Adult and juvenile mice of either sex were used. Their ages ranged between postnatal
 137 day (P) 2-12 or P25-60. The Chrb3-Cre transgenic mouse line, described previously (Drayson
 138 & Triplett, 2019), was obtained (MMRRC 036469-UCD) and genotyped with two primers against
 139 Cre (GTC-CAA-TTT-ACT-GAC-CGT-ACA-CC and GTT-ATT-CGG-ATC-ATC-AGC-TAC-ACC).
 140 Mice harboring a floxed allele of the Grin1 gene (GluN1^{flox}) and GCaMP5-IRES-tdTomato
 141 reporter mice were generated and genotyped as described previously (Tsien et al., 1996; and
 142 Gee et al., 2014). All animals were housed in the research animal facility at Children's National
 143 Research Institute, and all experimental procedures were approved by the Institutional Animal
 144 Care and Use Committee.

146 *Immunohistochemistry*

147 Mice were anesthetized on ice (< P8) or with halothane (2-bromo-2-chloro-1,1,1-
 148 trifluoroethane) (>P9) and transcardially perfused with ice-cold phosphate-buffered saline (PBS)
 149 followed by 4% paraformaldehyde (PFA) (pH 7.4). Brains and eyes were dissected and post-
 150 fixed in 4% PFA at 4°C overnight or 30 min, respectively. After post-fixation, brains and eyes
 151 were briefly washed in PBS before cryoprotection in 30% (brains) or 10% (eyes) sucrose at 4°C
 152 for 24-48 hrs. Tissues were then embedded in O.C.T. compound (Tissue-Tek 4583) and cooled
 153 in a -80°C freezer prior to being sectioned with ThermoScientific Micron HM 525 cryostat.
 154 Sections of 20 µm (brain) and 14 µm (eye) were collected directly onto SuperFrost Gold Plus
 155 microscopy slides (Fisher Scientific) and dried overnight at room temperature. Sections were
 156 incubated in blocking solution (1% serum, 0.25% Triton X-100) for 1 hour at room temperature
 157 and then incubated with primary antibodies diluted in blocking solution at 4°C overnight. The
 158 following primary antibodies were used: Anti-Beta 3 (Santa Cruz SC-6045, RRID: AB_2065343),
 159 Anti-Brn-3a (Santa Cruz SC-31984, RRID: AB_2167511), Anti-Calretinin (Millipore AB1550,

160 RRID: AB_90764), Anti-RBPMS (PhosphoSolutions 1830-RBPMS, RRID: AB_2492225), and
 161 Anti-Satb2 (ABcam AB34735, RRID: AB_2301417). Sections were washed thoroughly in PBS
 162 and then incubated with appropriate secondary antibodies (Biotium, RRIDs: AB-2534102, AB-
 163 162543) and DAPI diluted in blocking solution for 1 hour at room temperature. Confocal images
 164 were acquired at 20X magnification with an Olympus FV1000 microscope, with an Olympus
 165 DP71 digital camera attached. Images were analyzed and processed with FIJI (Schindelin et al.,
 166 2012). For each genotype, we averaged the number of counted cells over three different retinal
 167 sections from each of three animals. Data were analyzed, and graphs were constructed with
 168 GraphPad Prism8. All error bars represent the standard error of the mean (SEM), and statistical
 169 analysis was determined using the Mann-Whitney Rank Sum test.

170

171 *In situ hybridization*

172 Tissue was collected and fixed as described above. Complementary DNA for GluN1
 173 [containing nucleotides 25296659-25298429 of the open reading frame (ORF)] was used to
 174 make antisense and sense digoxigenin-labeled RNA probes and recognize exons 11 to 16.
 175 Slides were pretreated with PBS at room temperature for 5 minutes to rehydrate the slides prior
 176 to being fixed with 4% PFA (pH 7.4) for 15 min. Slides were also pretreated with proteinase K (1
 177 µg/mL) to increase hybridization efficiency. Prior to being treated with the RNA probe, slides had
 178 300 µL of hybridization buffer (50% formamide, 5X SSC pH: 4.5, 1% SDS, 50 µg/mL yeast
 179 tRNA, 50 µg/mL heparin) covered with parafilm, and incubated at 70°C for 1 hour. RNA probes
 180 were diluted 1:200 in hybridization buffer and placed onto the slides, covered with parafilm, and
 181 incubated at 70°C overnight. Slides were washed and blocked with TBST/HISS (1X TBS, 1%
 182 Tween-20, and 5% HISS) for 1 hour at RT. Antibodies against DIG were diluted (1:2000) in
 183 TBST/HISS, and 200µL was placed on each slide for 4°C overnight. Slides were then washed
 184 four times for 15 minutes with TBST and then washed with NTMT 3 times for 5 minutes. Slides

185 were then treated with 200 μ L of BMPurple (Roche) and developed for 12 hours at RT. Images
 186 were acquired at 4X, 10X, and 20X magnifications with a brightfield Olympus BX61 microscope.

187

188 *Quantitative PCR*

189 Total RNA was isolated from micro-dissected SC and the whole retina using the Aurum
 190 Total RNA Fatty and Fibrous Tissue Kit (Bio-Rad #7326830). Synthesis of cDNA was carried
 191 out using the iScript Reverse Transcription Supermix for RT-qPCR (Bio-Rad). qPCR was
 192 performed on a CFX96 real-time system (Bio-Rad #1708890) in a 20- μ L reaction mixture using
 193 SsoAdvanced Universal SYBR Green PCR master mix (Bio-Rad). Cycle parameters were 3 s at
 194 95 °C and 30 s at 60 °C. Data were normalized to housekeeping gene 18S. GluN1 primers: 5'-
 195 CCAGATGTCCACCAGACTAAA -3' and 5'-CCATTGACTGTGAACTCCTCTT-3' (Set 1), 5'-
 196 AAGGAGTGGAAACGGAATGATG-3' and 5'-GGCTTGGAGAACTCTATGTACTG-3' (Set 4), 5'-
 197 GTAGCTGGGATCTTCCTCATTT-3' and 5'-TTCTTCCTCCACACGTTTAC-3' (Set 5). 18S
 198 primers: 5'-CTTTGTCAAGCTCATTTCTGG-3' and 5'-TCTTGCTCAGTGTCTTGC-3'. Data
 199 were analyzed using the comparative CT method, and graphs were constructed with GraphPad
 200 Prism8 (Schmittgen & Livak, 2008). All error bars represent the SEM, and statistical analysis
 201 was determined using an unpaired student t-test.

202

203 *Anterograde RGC axon labeling*

204 Adult mice (P25-60) were anesthetized by intraperitoneal injection with a
 205 ketamine/xylazine cocktail (100/10 mg/kg). Additionally, adult mice were given Buprenex (0.3
 206 mg/kg) for analgesia. Pups (P0-P10) were anesthetized on ice. For focal or bulk labeling of
 207 RGCs, a 10% solution of lipophilic dye Dil (1,1'-dioctodecyl-3,3,3',3'-
 208 tetramethylindocarbocyanine perchlorate) in dimethylformamide (DMF) or a 2% solution of
 209 cholera toxin subunit B (CTB) 488 and 555 in PBS, respectively, was injected using a pulled-
 210 glass micropipette attached to a Picospritzer III (Parker-Hannifin). The glass micropipette was

211 inserted into the retina of the anesthetized animal, and ~100 nL of Dil solution was injected into
 212 one eye or ~500 nL CTB-488 was injected into the left eye, and CTB-555 was injected into the
 213 right eye. Animals recovered for 1 week (adults) or 2 days (pups) before being euthanized and
 214 their brains post-fixed in 4% PFA overnight as described above. The termination zone (TZ) of
 215 Dil-labeled RGCs was visualized in whole mount via epifluorescent microscopy. Brains were
 216 then embedded in 2-3% agarose and sectioned coronally at 150 microns on a vibratome. The
 217 dLGN and SC were visualized at 1.25X magnification via epifluorescent microscopy and
 218 analyzed using FIJI.

219

220 *Image analysis*

221 To determine topographic refinement of TZs, we calculated a termination zone index
 222 (TZI), for which the size of the TZ in the SC or dLGN, expressed as a percent of the target area,
 223 was divided the injection size, expressed as a percent of the flat-mounted retina. For the dLGN,
 224 we quantified the TZI for all sections containing the TZ and determined an average across
 225 sections for each animal. The TZIs were statistically analyzed by running a student's t-test with
 226 GraphPad Prism8. To assess eye-specific segregation, each coronal section that contained
 227 labeled retinal terminals **was** assessed independently using FIJI, and the average across all
 228 sections was used. The boundaries of the dLGN/SC were outlined on a grayscale 8-bit image,
 229 and the background was cleared before measuring the size of the dLGN/SC. The areas of
 230 ipsilateral and contralateral retinal innervation were determined independently, and the
 231 overlapping co-localized pixels were then analyzed using the 'AND' function of FIJI's image
 232 calculator. The measurement of the overlap/**ipsi area, overlap/total dLGN, and ipsi patch**
 233 **length** was then statistically analyzed by running a student's t-test or 2-way ANOVA with
 234 GraphPad Prism8 for adult and developmental ages, respectively. All error bars represent SEM.
 235 **Outliers were identified by running a Grubb's test (outlier test) with GraphPad's Outlier**
 236 **Calculator and removed from analysis.**

237

238 *Acute brain slice preparation*

239 Chrb3-Cre;GCaMP5-tdTomato pups aged P2-6 of either sex were used. Pups were
 240 decapitated, and the brains were rapidly removed and immersed in ice-cold cutting solution (230
 241 mM sucrose, 2.5 mM KCl, 0.5 mM CaCl_2 , 10 mM MgCl_2 , 26 mM NaHCO_3 , 1.25 mM NaH_2PO_4 ,
 242 0.04 mM Na-Ascorbate, and 10 mM glucose, pH 7.2 to 7.4). Coronal and sagittal slices (300
 243 μm) were cut with a vibratome (Leica VT1000S) and transferred to artificial cerebral spinal fluid
 244 (aCSF) (126 mM NaCl, 4 mM KCl, 2 mM CaCl_2 , 1 mM MgCl_2 , 26 mM NaHCO_3 , 1.25 mM
 245 NaH_2PO_4 , 0.04 mM Na-Ascorbate, and 10 mM glucose, pH 7.2 to 7.4, osmolarity = 310
 246 mOsm/L) bubbled with 95% O_2 and 5% CO_2 or into MgCl_2 -free aCSF (126 mM NaCl, 4 mM KCl,
 247 2 mM CaCl_2 , 26 mM NaHCO_3 , 1.25 mM NaH_2PO_4 , 0.04 mM Na-Ascorbate, and 10 mM glucose,
 248 pH 7.2 to 7.4, osmolarity = 310 mOsm/L) bubbled with 95% O_2 and 5% CO_2). Slices recovered
 249 in oxygenated aCSF for 1 hour at room temperature (21° to 25°C) before acute slice imaging.
 250 During recordings, slices were placed in a perfusion chamber and superfused with oxygenated
 251 aCSF at room temperature for the duration of the experiment. The cells were visualized with a
 252 20X immersion objective (Olympus Optical, New York, NY) and epifluorescence.

253

254 *Ca^{2+} imaging and analysis*

255 Ca^{2+} imaging was performed with an Olympus (Tokyo, Japan) FluoView FVMPE-RS
 256 Multiphoton Microscope imaging system using FluoView software and a Ti:Sapphire laser
 257 source emitting 140 fs pulses at an 80 MHz repetition rate with a wavelength adjustable for 690-
 258 1040 nm (Maitai DeepSee pulsed, infrared laser). Full-field of view images **were** acquired with
 259 XY raster scanning using the 20X 0.95 NA water-immersion objective. Changes in fluorescence
 260 (ΔF) was quantified using ImageJ (NIH) software and expressed as a percentage of baseline
 261 ($\%\Delta F/F$). Time-lapse images of neuron Ca^{2+} signaling were recorded at a frame rate of 1Hz.
 262 ROIs will be selected based on the appearance of GCaMP5G Ca^{2+} transients in the time-lapse

263 images. To trigger Ca^{2+} transients, the agonist NMDA (50 μM) and control K^+ (mM) were
264 dissolved in aCSF and delivered locally by a pressure pulse (10 psi; 100-500 ms) using a
265 Picospritzer III (Parker Instrumentation, Chicago, IL) while the antagonist MK-801 (10 μM) was
266 delivered via bath perfusion. To avoid potential artifacts due to K^+ administration, it was always
267 the last agent tested in any given slice. Data were analyzed, and graphs were constructed with
268 GraphPad Prism8. All error bars represent the SEM, and statistical analysis was determined
269 using a one-way ANOVA followed by Tukey's multiple comparisons test, as indicated in the
270 figure legend. ** $p < 0.01$, **** $p < 0.0001$, Not Significant (N.S.) $p > 0.05$.

271 Results

272 RGC-specific loss of *GluN1* expression in *Chrn3-Cre;GluN1^{flox/flox}* mice

273 To study the RGC-specific role of NMDAR function during topographic map formation,
 274 we took a conditional genetic approach. We crossed the *Chrn3-Cre* line, in which Cre
 275 recombinase is expressed broadly by RGCs but not in retinorecipient areas such as the SC or
 276 dLGN (Drayson & Triplett, 2019), with a line harboring a floxed allele of the *Grin1* gene coding
 277 for the GluN1 subunit of the NMDAR (*GluN1^{flox}*), in which exon 11 through the 3' end are flanked
 278 by loxP sites (Tsien et al., 1996) to generate pre-cKO mice. Previous reports suggest that
 279 recombination of this locus results in the complete loss of NMDAR function (Tsien et al., 1996).

280 In the transgenic *Chrn3-Cre* mouse line, the majority of expression is observed in the
 281 ganglion cell layer (GCL) and distributed broadly across the retina (Drayson & Triplett, 2019).
 282 Indeed, we observed that when *Chrn3-Cre* mice are crossed with β -galactosidase (LacZ) and
 283 tdTomato (tdTom) reporter lines, LacZ expression is observed throughout the retina (Fig. 1A),
 284 and tdTom expression is restricted to the GCL (Fig. 1B). In order to determine if our genetic
 285 strategy was valid, we performed RNA *in situ* hybridization for *GluN1* mRNA in P4 retinal tissue.
 286 In control retinas (from mice that were genotyped as Cre⁻ and either *GluN1^{fl/+}* or *GluN1^{fl/fl}*, [Ctl]),
 287 the *GluN1* anti-sense probe produced a strong signal in cell bodies throughout the GCL and INL
 288 (Fig. 1C). These findings are consistent with previous reports in which nearly all RGCs
 289 expressed the GluN1 subunit (Brandstätter et al., 1994). Strikingly, little to no *GluN1* mRNA
 290 expression was detected in the retinas of P4 pre-cKO mice (Fig. 1D), suggesting we were able
 291 to successfully ablate GluN1 from the GCL in our experimental animals during the first postnatal
 292 week. However, some GluN1 expressing cells in the GCL and IPL were observed (Fig. 1D
 293 arrowhead); these cells may be the small population of RGCs not targeted in the *Chrn3-Cre*
 294 line or displaced amacrine cells (Drayson and Triplett, 2019). Notably, signal from the *GluN1*
 295 anti-sense mRNA probe did label cell bodies throughout the SC of both Ctl and pre-cKO brains
 296 (Fig. 1E & F), suggesting NMDAR function remains intact in this region.

297 To further demonstrate that *GluN1* expression was reduced in pre-cKO retinas, we
 298 performed RT-qPCR comparing the SC and retina of Ctl and pre-cKO animals at P0 using three
 299 primer sets (Fig. 1H & I). Primer set 1 is located at exon 9, upstream of the flanking site of the
 300 *GluN1* gene. Primer set 4 is located near exon 12, just after the flanking site. Primer set 5 is
 301 located near exon 19, towards the end of the *GluN1* gene (Fig. 1G). This analysis confirmed
 302 that our pre-cKO animal had a knockdown of *GluN1* expression in the retina with both set 4 and
 303 5 (Set 4 Ctl: 1.020 ± 0.09136 , $n = 6$; Set 4 pre-cKO: 0.4604 ± 0.03565 , $n = 8$; $p < 0.001$,
 304 student's t-test; Set 5 Ctl: 1.007 ± 0.05547 , $n = 6$; Set 5 pre-cKO: 0.1029 ± 0.04445 , $n = 8$; $p <$
 305 0.001 , student's t-test) (Fig. 1H). As expected, we saw no change in relative expression when
 306 analyzing primer set 1, since the region amplified by this set was not ablated (Set 1 Ctl: 0.8573
 307 ± 0.03889 , $n = 6$; Set 1 pre-cKO: 0.9283 ± 0.04024 , $n = 8$; $p = 0.2134$, student's t-test) (Fig. 1I).
 308 Additionally, the qPCR analysis with all three primer sets confirmed that *GluN1* expression was
 309 unchanged in the SC (Set 1 Ctl: 0.8259 ± 0.05876 , $n = 6$; Set 1 pre-cKO: 0.7911 ± 0.07140 , $n =$
 310 8 ; $p = 0.8876$, student's t-test; Set 4 Ctl: 0.7815 ± 0.07300 , $n = 6$; Set 4 pre-cKO: $0.8136 \pm$
 311 0.04889 , $n = 8$; $p = 0.9100$, student's t-test; Set 5 Ctl: 0.8128 ± 0.08384 , $n = 6$; Set 5 pre-cKO:
 312 0.6149 ± 0.08005 , $n = 8$; $p = 0.0954$, student's t-test) (Fig. 1H). Together, these data indicate
 313 neurons in the GCL of the retina express *GluN1* during developmental stages and demonstrate
 314 this expression is dramatically reduced in pre-cKO retinas, but not the SC.

315

316 *Cytoarchitecture of the retina is unaffected in the absence of GluN1 expression in RGCs*

317 Previous studies suggest a critical role for NMDA signaling in the survival of RGCs
 318 (Shen et al., 2006). Thus, we wanted to determine if RGC-specific deletion of *GluN1* altered the
 319 number of RGCs or morphological organization of the retina. To begin, we performed
 320 immunohistochemistry for markers of different retinal cell types. First, we analyzed the RGC
 321 markers RBMPS and Brn3a, since a substantial proportion of Chrb3-Cre-tagged RGCs
 322 expresses Brn3a (Drayson & Triplett, 2019) (Fig. 2A-B & F-G). The number of RBPMS labeled

323 cells in a 500 x 500 μm field of the retina for pre-cKO animals (258.7 ± 10.48 , $n = 3$) was not
 324 significantly different from controls (263.0 ± 9.644 , $n = 3$) ($p > 0.9999$, Mann-Whitney test) (Fig.
 325 2K). The number of Brn3a labeled cells in a 500 x 500 μm field of the retina for pre-cKO animals
 326 (122.7 ± 5.239 , $n = 3$) was not significantly different from controls (119.3 ± 5.783 , $n = 3$) ($p >$
 327 0.9999 , Mann-Whitney test) (Fig. 2L). Similarly, we detected no significant difference in the
 328 number of cells labeled with SatB2, a putative marker of direction-selective RGCs (Sweeney et
 329 al., 2019) (Ctl: 68.0 ± 1.732 , $n = 3$; pre-cKO: 73.0 ± 2.082 , $n = 3$; $p = 0.2000$, Mann-Whitney
 330 test) (Fig. 2M). In order to further examine the morphology of the retina, we stained for Beta3, a
 331 marker for Off bipolar cells, and calretinin, which labels a variety of amacrine cells and RGCs,
 332 including their processes in the inner plexiform layer. As with RBPMS, Brn3a and SatB2, we
 333 found no significant difference in number of cells expressing Beta3 nor calretinin between
 334 control and pre-cKO retinas (Beta 3 Ctl: 163.0 ± 7.371 , $n = 3$; Beta3 pre-cKO: 155.3 ± 15.24 , n
 335 $= 3$; $p > 0.9999$, Mann-Whitney test; calretinin Ctl: 134.7 ± 7.767 , $n = 3$; calretinin pre-cKO:
 336 134.7 ± 3.512 , $n = 3$; $p > 0.9999$, Mann-Whitney test) (Fig. 2D-E, I-J, & N-O). Further, the
 337 organization of Beta3 and calretinin-stained processes in the inner plexiform layer in pre-cKO
 338 retinas were grossly organized similarly to those in Ctl retinas. Overall, these data suggest **that**
 339 **neither** the population of RGCs nor cytoarchitecture of the retina is adversely impacted due to a
 340 loss of NMDAR function in RGCs.

341

342 *Expression of the GluN1 subunit of the NMDAR in RGCs is not required in topographic* 343 *refinement*

344 We next tested our hypothesis that NMDAR expression in RGCs is required for the
 345 establishment of retinofugal topography utilizing the focal Dil tracing technique in adult animals
 346 (P25-60), as previously described (Kay et al., 2018). In every animal, the axonal projections
 347 from the focal Dil injection into the retina showed a topographically appropriate termination zone

(TZ) in the SC of adult Ctl and pre-cKO mice (Fig. 3A & B). Previous studies in which NMDAR function was disrupted pharmacologically suggested that while labeled RGCs terminate in roughly the appropriate topographic zone, the size of the termination field was increased (Simon et al., 1992). To determine if TZ size was altered in pre-cKO mice, we calculated the termination zone index (TZI) by normalizing the TZ size by the injection site size. We observed no change in TZI in mice lacking GluN1 in RGCs (TZI: Ctl: 8.806 ± 2.738 , $n = 6$; pre-cKO: 11.13 ± 3.597 , $n = 9$; $p = 0.6481$, student's t-test) (Fig. 3C). Further, we did not observe stray arbors that might indicate subtle deficits not detectable by quantification of TZI (Fig. 3A' & B'). These data suggest NMDAR function in RGCs is not required for retinocollicular refinement.

In addition to the SC, RGCs project topographically to the dLGN, where spontaneous activity plays a critical role in establishing topography, **along with** molecular cues (Pfeifferberger et al., 2006). Therefore, in addition to testing the retinocollicular refinement of our transgenic animals, we observed the retinogeniculate refinement within the same Dil injected animals. **Topographic refinement was not significantly altered, though there appeared to be a trend toward a reduction in TZI in pre-cKO animals** (TZI: Ctl: 6.229 ± 1.308 ; pre-cKO: 3.141 ± 0.6921 ; $p = 0.0520$, student's t-test) (Fig. 3D-F). Together, these data suggest expression of GluN1 in RGCs is not required for the development of retinogeniculate map refinement.

Eye-specific segregation in the SC and dLGN

While retinofugal topography appeared unchanged in the absence of GluN1 expression in RGCs, we reasoned that other developmental processes in visual circuit development that are more reliant on activity-dependent mechanisms may be altered. The segregation of eye-specific inputs in visual areas has served as a classical model to demonstrate the role of both spontaneous activity and visual experience in circuit development and plasticity (Feller, 2009). Indeed, it has been established that during eye-specific segregation in the LGN, large-scale

refinement takes place. Glutamatergic waves generated in the retina are critical for maintenance of segregation (Demas et al., 2006), and NMDAR blockade in *in vitro* preparations alters the frequency of glutamatergic waves, but not other attributes, such as velocity (Blankenship et al., 2009). Further, NMDARs have been implicated in the segregation of artificially-induced eye-specific inputs in the frog tectum (Cline & Constantine-Paton, 1990).

In order to determine if the expression of GluN1 in RGCs is critical for appropriate eye-specific segregation, we intraocularly injected fluorescently-labeled cholera toxin B subunit (CTB)-488 in the left eye and CTB-555 in the right eye and observed their terminations in the dLGN. As expected, in both control and pre-cKO adults, the majority of the dLGN was occupied by contralateral projections except for the dorsomedial region where the ipsilateral projections terminate (Fig. 4A-F). We analyzed eye-specific segregation by calculating the area of overlap between contralateral and ipsilateral projections in relation to the area occupied by ipsilateral projections and found no significant difference between control and pre-cKO adult mice (Overlap/Ipsi: control: 34.18 ± 2.958 , $n=11$; pre-cKO: 38.08 ± 2.172 , $n=10$; $p = 0.3090$, student's t-test) (Fig. 4G).

Next, we analyzed the overlap in the SC of these animals and found that eye-specific segregation was not significantly different between the SCs of pre-cKO and control adult animals (Overlap/Ipsi: Ctl: 2.382 ± 0.2595 , $n=11$; pre-cKO: 2.004 ± 0.2784 , $n=10$; $p = 0.3320$, student's t-test) (Fig. 5A-C). Although eye-specific segregation is heavily dependent on activity, these data suggest GluN1 expression in RGCs is not required in order to achieve the mature segregation of eye-specific inputs in the LGN, consistent with previous studies (Hahm et al., 1991; Smetters et al., 1994).

We next wondered if the developmental trajectory of eye-specific segregation might be altered in the absence of GluN1 expression in RGCs. We tested this possibility by analyzing the overlap of contralateral and ipsilateral projections in pups (P2-P12) (Fig. 6). At P4, the retinogeniculate axons from the two eyes are not well separated, as expected (Fig. 6A & D).

400 However, over time, eye-specific segregation became more and more refined by the end of the
 401 second post-natal week (Fig. 6B-C & E-F). As expected, we found a main effect of age in the
 402 amount of overlap between ipsi- and contra-RGC terminals in the dLGN, **when calculated as a**
 403 **proportion of the ipsi-RGC domain** ($p < 0.0001$, 2-way ANOVA). Interestingly, we found that
 404 overlap was different between each age group ($p < 0.05$, Tukey's multiple comparisons test)
 405 except for between P6 and P8 ($p = 0.7511$). These data suggest paradoxical increases in
 406 overlap from P2 to P4 and P10 to P12 in our dataset, but the general trend is a decrease in
 407 overlap over time, consistent with previous data (Pfeifferberger et al., 2005). However, we did
 408 not find any effect of genotype ($p = 0.1657$, 2-way ANOVA) nor any interaction between age
 409 and genotype ($p = 0.1516$, 2-way ANOVA) (Fig. 6G). **We next wondered if the increase in**
 410 **overlap was due to changes in the size of the ipsi-RGC domain in the dLGN. To do so, we**
 411 **calculated the amount of overlap of ipsi- and contra-RGC terminals as a proportion of the**
 412 **total size of the dLGN. Again, we observed a main effect of age** ($p < 0.0001$, 2-way
 413 ANOVA), but found no effect of genotype ($p = 0.4183$) nor any interaction between age
 414 and genotype ($p = 0.1981$) (Fig. 6H). Interestingly, we found significant differences
 415 between all age groups ($p < 0.0001$, Tukey's multiple comparisons test) except when
 416 comparing P6 to P8 ($p = 0.6827$) and P10 to P12 ($p = 0.1773$). Lastly, we analyzed the
 417 ipsilateral patch length over the length of the dLGN (Fig. 6I). Similar to our analyses of
 418 overlap, we found a main effect of age ($p < 0.0001$, 2-way ANOVA), but not genotype ($p =$
 419 **0.8871**) nor any interaction the two ($p = 0.6740$). For this metric, we found significant
 420 differences when comparing P2 or P4 to all ages ($p < 0.05$), when comparing P6 to P10
 421 and P12 ($p < 0.05$), and a trend towards a difference when comparing P6 to P8 ($p =$
 422 **0.0740**). Altogether, these data suggest NMDAR activity in RGCs is not required for the
 423 development or maintenance of eye-specific segregation, **but reveal age-dependent effects**
 424 **on eye-specific segregation.**

425

426 *Activation of NMDA-mediated response in RGC terminals in retinorecipient areas*

427 Thus far, our data suggest that retinofugal development is not dependent on NMDAR
428 expression in RGCs. One possibility for this could be that pre-synaptic NMDARs may not be
429 located in the terminals of RGCs in these retinorecipient centers, contrary to what has been
430 suggested in the frog tectum (Kesner et al., 2020). To test this, we crossed the *Chrn3-Cre* line
431 with Cre-dependent *GCaMP5G::tdTom* reporter mice (Gee et al., 2014) and performed Ca^{2+}
432 imaging in retinorecipient areas, where only RGC terminals would be labeled. We began by
433 testing the activity of RGC axons in the SC with NMDA at 50mM and 100mM, and found that an
434 elicited calcium response could be visualized in Mg^{2+} -free aCSF, but not in aCSF (Fig. 7A-C &
435 E) (NMDA in Mg^{2+} -free aCSF: 28.48 ± 3.962 , $n = 6$; NMDA in aCSF: -3.907 ± 0.9898 , $n = 5$, $p <$
436 0.0001 , Tukey's *post hoc* test). Importantly, this response was significantly smaller than that
437 observed when we administered 5mM K^{+} stimulation as a positive control (Fig. 7D & E) (K^{+}
438 stimulation in aCSF: 44.10 ± 1.482 , $n = 3$, $p = 0.0060$, Tukey's *post hoc* test), suggesting that
439 NMDA application was not driving wholesale activation of RGCs, but rather specific activation of
440 NMDARs on RGC terminals. Indeed, when we administered 50mM and 100mM of NMDA in the
441 presence of the specific NMDAR antagonist, MK-801, the calcium response was ablated (Fig.
442 7C & E) (NMDA in Mg^{2+} -free aCSF + MK-801: 3.057 ± 0.3887 , $n = 6$, $p < 0.0001$, Tukey's *post*
443 *hoc* test). We observed a similar pattern of activation of RGC terminals in the dLGN (data not
444 shown), consistent with previous data demonstrating that most RGCs that project to the dLGN
445 also project to the SC (Dhande et al., 2011). Overall, these data suggest that NMDA-mediated
446 activity is elicited by direct stimulation of RGC terminals in the SC, supporting the presence of
447 pre-synaptic NMDARs at retinocollicular synapses.

448 Discussion

449 During the development of the visual system, RGCs undergo extensive remodeling
450 mediated by a combination of molecular cues, axon-axon competition and neuronal activity in
451 order to develop precise terminations in retinorecipient regions. Spontaneous activity in the form
452 of retinal waves helps ensure retinocollicular and retinogeniculate refinement; however, the
453 specific mechanisms by which activity mediates these processes remain unclear. Here, we
454 tested the role of NMDARs expressed by RGCs in the development of precise retinofugal
455 projection organization in the mouse. We found that our novel conditional genetic approach
456 successfully ablated NMDARs from RGCs without altering gross retinal organization or
457 expression in the SC. Anatomical tracing experiments revealed no changes in topographic
458 refinement nor eye-specific segregation in either the SC or dLGN. This is the case despite the
459 fact that we observed NMDA-elicited Ca^{2+} transients in RGC terminals in retinorecipient regions.
460 Together, these data demonstrate that NMDARs expressed by RGCs are not required for
461 topographic refinement nor eye-specific segregation in image-forming retinorecipient regions

463 *NMDARs expressed by RGCs are not required for retinotopy*

464 Previous studies demonstrated that neuronal activity mediated through NMDARs plays
465 an important role in establishing the topography of retinocollicular projections. When NMDARs
466 were chronically blocked during SC development, mRNA levels of GluN1 are decreased (Hofer
467 et al., 1994); additionally, proper activity level of NMDARs is required for the appropriate
468 development and refinement of the retinofugal map (Cline & Constantine-Paton, 1989; Simon et
469 al., 1992; King et al., 1996; and Mize & Butler, 2000). Further, terminal arbors of RGCs in the
470 optic tectum exhibit robust dynamics, which are disrupted when NMDAR function is blocked
471 (Rajan et al., 1999; Ruthazer et al., 2003; Munz et al., 2014). And NMDARs play a critical role in
472 the plasticity required for synaptic convergence following map compression in the SC (Huang &
473 Pallas, 2001). However, these pharmacological studies could not distinguish between potential

474 contributions of pre-synaptic or post-synaptic NMDAR activity in these processes, each of which
 475 have been implicated in plasticity in other brain regions (Paoletti et al., 2013).

476 To overcome this limitation, we developed a conditional knockout model to directly
 477 determine if NMDARs expressed by RGCs play a role in map formation. In the SC of pre-cKO
 478 mice, we did not observe alterations in the size of TZs from labeled RGCs, demonstrating that
 479 NMDARs expressed by these neurons are not required for topographic refinement in this region.
 480 Interestingly, these data are somewhat inconsistent with recent work in which sparser
 481 retinotectal terminals were observed when GluN1 expression was knocked down specifically in
 482 RGCs (Kesner et al., 2020). However, the total size of the terminal arbor may have been less
 483 dramatically impacted, as no change was observed in total terminal branch length. This result is
 484 consistent with previous studies leveraging pharmacologic NMDAR blockade, in which
 485 disruptions of RGC axonal arbor dynamics were observed (Rajan et al., 1999; Ruthazer et al.,
 486 2003; Munz et al., 2014), but the overall mature organization of arborizations was not
 487 dramatically altered (Cline & Constantine-Paton, 1989). Indeed, functional analyses revealed no
 488 changes in overall receptive field size when GluN1 expression was knocked down in RGCs,
 489 consistent with minimal change in topography (Kesner et al., 2020). One possible reason for a
 490 lack of phenotype in terms of topographic refinement may be that the Cre line chosen is
 491 expressed in only ~65% of RGCs (Drayson & Triplett, 2019). However, our qPCR data suggest
 492 a substantial knockdown of all retinal expression of *GluN1*, suggesting that the vast majority of
 493 RGCs lack expression in this model. **Intriguingly, we did observe a trend towards a**
 494 **decreased TZI for retinogeniculate projections, which would be consistent with sparser**
 495 **terminals reported for retinotectal projections lacking NMDARs in RGCs (Kesner et al.,**
 496 **2020). This raises the intriguing possibility that pre-synaptic NMDARs may play distinct**
 497 **roles in circuit formation in the SC and dLGN. However, more sophisticated analyses of**
 498 **retinal convergence in the SC and dLGN are needed to draw firm conclusions regarding**
 499 **the context-dependent roles of pre-synaptic NMDARs.**

500

501 *NMDARs in RGCs are not required for eye-specific segregation*

502 The establishment of eye-specific organization in the visual system has served as a
503 model to understand the mechanisms underlying circuit development and plasticity (Hensch &
504 Quinlan, 2018; and Arroyo & Feller, 2016). Intriguingly, previous studies in which eye-specific
505 segregation was induced in the context of retinotectal projections in frogs (Constantine-Paton &
506 Law, 1978) suggested activation or inhibition of NMDAR function could enhance or disrupt
507 segregation, respectively (Cline & Constantine-Paton, 1990). Here, we found no changes in the
508 mature organization of eye-specific lamina in the SC nor dLGN when NMDAR function was
509 disrupted in RGCs. **Although, as noted for the lack of phenotype observed for**
510 **retinocollicular projections, the fact that not all RGCs are targeted in Chrn3-Cre mice**
511 **could mask a potential role for pre-synaptic NMDARs in eye-specific segregation.** Further,
512 we did not observe alterations in the developmental trajectory of segregation in the dLGN
513 between genotypes **in any of our analyzed parameters.** Interestingly, we did observe
514 increases in overlap **as a percent of the ipsi-RGC domain** from P2 to P4 and P10 to P12. **The**
515 **increased overlap from P2 to P4 may be driven by the fact that ipsi-RGC innervation of**
516 **the dLGN is not complete until P4 (Godement et al., 1984). One explanation for the**
517 **increase overlap observed between P10 to P12 could be a reduction in the number ipsi-**
518 **RGC prior to eye opening. Indeed, when we analyzed overlap as a proportion of the size**
519 **of the dLGN, we did not observe significant differences between P10 and P12. However,**
520 **we found that the size of the ipsi-RGC patch, as measured by its length, decreased until**
521 **P8, but not thereafter. Together, these data support a slight reversal of eye-specific**
522 **segregation just before eye-opening, which could be masked depending on the method**
523 **of quantification.** Of note, many investigations of eye-specific segregation in the mouse dLGN
524 did not sample with the frequency that we did (every two days) (Jaubert-Miazza et al., 2005;
525 Muir-Robinson et al., 2002; Demas et al., 2006). One study that sampled with the same

frequency did not report overlap at P2 or P12 (Pfeiffenberger et al., 2005). Thus, the changes we observe may reflect a high degree of dynamics in eye-specific sorting in the mouse dLGN. Though it is important to note that the changes we observed were small, and the general trend was consistent with these previous studies.

In addition to roles in synaptic plasticity, axonal refinement, and arbor stabilization, NMDARs have also been implicated in the generation of glutamatergic waves, which play a critical role in the maintenance of eye-specific segregation (Cline & Constantine-Paton, 1989; Iwasato et al., 1997; Ruthazer & Cline, 2004; Hu et al., 2005; Demas et al., 2006; Munz et al., 2014). Indeed, NMDAR blockade in *in vitro* preparations alters the frequency of glutamatergic waves, but not other attributes, such as velocity (Blankenship et al., 2009). These results raise the possibility that disruption of NMDAR expression in RGCs might alter the pattern of glutamatergic waves. While we did not monitor these waves directly, the lack of an eye-specific segregation phenotype observed in pre-cKO mice, both in the mature and developing state, suggests NMDARs in RGCs are dispensable for the wave-dependent information mediating maintenance of segregation. Indeed, these findings are consistent with recent work elucidating a role for NMDARs on the pre-synaptic side of bipolar cell terminals in the initiation and propagation of glutamatergic waves (Zhang, et al., 2016a).

NMDARs may be present on developing RGC terminals

The lack of disruptions in topography and eye-specific segregation we observed in pre-cKO mice raised the question of whether, in fact, NMDARs are localized and functional in terminals of developing RGCs. The expression pattern of NMDARs in the developing brain has been difficult to examine due to a lack of suitable antibodies for immunolocalization of the obligate GluN1 subunit. While, recent studies suggest NMDARs are expressed in both the cell bodies and dendrites of RGCs (Zhang, et al., 2016b), the successful labeling of NMDARs on axons or at terminals has not been reported in murine models. To explore the possibility of

552 NMDARs located pre-synaptically in murine RGC terminals, we used combination Chrb3-
553 Cre;GCaMP5::TdTom mice. This animal model allows us to not only visualize RGC terminals in
554 slices through retinorecipient regions, but it also restricts Ca^{2+} indicator expression to RGC
555 terminals. Using this methodology, we observed Ca^{2+} transients in RGC terminals in both the
556 dLGN and the SC, which were ablated in the presence of the NMDAR-specific antagonist, MK-
557 801. These data suggest that NMDARs are localized pre-synaptically. However, the possibility
558 that indirect activation of RGC terminals occurs via administration of NMDA cannot be ruled out,
559 as the temporal dynamics of GCaMP are too slow to resolve this. However, the presence of
560 axo-axonal synapses onto RGCs that could lead to such a result have not been reported to our
561 knowledge.

562

563 *Conclusion*

564 Here, we have utilized a conditional genetic knockout method to probe the role of
565 NMDARs expressed by RGCs in the development of ordered connectivity in image-forming
566 retino-recipient nuclei. We did not observe alterations in either topography or eye-specific
567 segregation in the SC or dLGN in pre-cKO mice, demonstrating that NMDARs in RGCs play a
568 minimal role in these processes. Further, using conditional expression of genetically-encoded
569 Ca^{2+} indicators in RGCs, we present evidence that NMDARs may be present in developing
570 RGC terminals in the mouse.

571

References

572

Ackman, J. B., et al. (2012). Retinal waves coordinate patterned activity throughout the

573

developing visual system. *Nature*, 490(7419), 219-225. doi:10.1038/nature11529

574

Aoki, C., et al. (1994). Cellular and subcellular localization of NMDA-R1 subunit

575

immunoreactivity in the visual cortex of adult and neonatal rats. *Journal of Neuroscience*,

576

14(9), 5202-5222. doi:10.1523/JNEUROSCI.14-09-05202.1994

577

Arroyo, D. A., & Feller, M. B. (2016). Spatiotemporal features of retinal waves instruct the wiring

578

of the visual circuitry. *Frontiers in Neural Circuits*, 10, 54. doi:10.3389/fncir.2016.00054

579

Blankenship, A. G., et al. (2009). Synaptic and extrasynaptic factors governing glutamatergic

580

retinal waves. *Neuron*, 62(2), 230-241. doi:10.1016/j.neuron.2009.03.015

581

Bouvier, G., et al. (2015). Presynaptic NMDA receptors: Roles and rules. *Neuroscience*, 311,

582

322-340. doi:10.1016/j.neuroscience.2015.10.033

583

Bouvier, G., et al. (2018). Towards resolving the presynaptic NMDA receptor debate. *Current*

584

Opinion in Neurobiology, 51, 1-7. doi:10.1016/j.conb.2017.12.020

585

Brandstätter, J. H., et al. (1994). *Expression of NMDA and high-affinity kainate receptor subunit*

586

mRNAs in the adult rat retina. Oxford] : Blackwell Science. doi:10.1111/j.1460-

587

9568.1994.tb00607.x

588

Cang, J., et al. (2008). Selective disruption of one cartesian axis of cortical maps and receptive

589

fields by deficiency in Ephrin-as and structured activity. *Neuron*, 57(4), 511-523.

590

doi:10.1016/j.neuron.2007.12.025

- 591 Chandrasekaran, A. R., et al. (2007). Developmental homeostasis of mouse retinocollicular
 592 synapses. *Journal of Neuroscience*, 27(7), 1746-1755. doi:10.1523/JNEUROSCI.4383-
 593 06.2007
- 594 Cline, H. T., & Constantine-Paton, M. (1990). NMDA receptor agonist and antagonists alter
 595 retinal ganglion cell arbor structure in the developing frog retinotectal projection. *Journal of*
 596 *Neuroscience*, 10(4), 1197-1216. doi:10.1523/JNEUROSCI.10-04-01197.1990
- 597 Cline, H. T., & Constantine-Paton, M. (1989). NMDA receptor antagonists disrupt the
 598 retinotectal topographic map. *Neuron*, 3(4), 413-426. doi:10.1016/0896-6273(89)90201-8
- 599 Constantine-Paton, M., & Law, M. I. (1978). Eye-specific termination bands in tecta of three-
 600 eyed frogs. *Science*, 202(4368), 639-641. doi:10.1126/science.309179
- 601 Corlew, R., et al. (2007). Developmental switch in the contribution of presynaptic and
 602 postsynaptic NMDA receptors to long-term depression. *Journal of Neuroscience*, 27(37),
 603 9835-9845. doi:10.1523/JNEUROSCI.5494-06.2007
- 604 Demas, J., et al. (2006). Failure to maintain eye-specific segregation in nob, a mutant with
 605 abnormally patterned retinal activity. *Neuron*, 50(2), 247-259.
 606 doi:10.1016/j.neuron.2006.03.033
- 607 Dhande, O. S., et al. (2011). Development of single retinofugal axon arbors in normal and $\beta 2$
 608 knock-out mice. *The Journal of Neuroscience*, 31(9), 3384-3399.
 609 doi:10.1523/JNEUROSCI.4899-10.2011
- 610 Drayson, L. E., & Triplett, J. W. (2019). A Chrnb3-Cre BAC transgenic mouse line for
 611 manipulation of gene expression in retinal ganglion cells. *Genesis*, 57(9), e23305-n/a.
 612 doi:10.1002/dvg.23305

- 613 Feldheim, D. A., & O'Leary, D. D. M. (2010). Visual map development: Bidirectional signaling,
 614 bifunctional guidance molecules, and competition. *Cold Spring Harbor Perspectives in*
 615 *Biology*, 2(11), a001768. doi:10.1101/cshperspect.a001768
- 616 Feller, M. B. (2009). Retinal waves are likely to instruct the formation of eye-specific
 617 retinogeniculate projections. *Neural Development*, 4(1), 24. doi:10.1186/1749-8104-4-24
- 618 Gee, J. M., et al. (2014). Imaging activity in neurons and glia with a Polr2a-based and cre-
 619 dependent GCaMP5G-IRES-tdTomato reporter mouse. *Neuron*, 83(5), 1058-1072.
 620 doi:10.1016/j.neuron.2014.07.024
- 621 Godement, P., et al. (1984). Prenatal and postnatal development of retinogeniculate and
 622 retinocollicular projections in the mouse. *Journal of Comparative Neurology* (1911), 230(4),
 623 552-575. doi:10.1002/cne.902300406
- 624 Hahm, J. O., et al. (1991). *Disruption of retinogeniculate afferent segregation by antagonists to*
 625 *NMDA receptors*. London] : Nature Pub Group. doi:10.1038/351568a0
- 626 Hensch, T. K., & Quinlan, E. M. (2018). Critical periods in amblyopia. *Visual Neuroscience*, 35,
 627 E014. doi:10.1017/S0952523817000219
- 628 Hofer, M., et al. (1994). Regulation of NMDA receptor mRNA during visual map formation and
 629 after receptor blockade. *Journal of Neurochemistry*, 62(6), 2300-2307. doi:10.1046/j.1471-
 630 4159.1994.62062300.x
- 631 Hu, B., et al. (2005). BDNF stabilizes synapses and maintains the structural complexity of optic
 632 axons in vivo. *Development (Cambridge)*, 132(19), 4285-4298. doi:10.1242/dev.02017

- 633 Huang, L., & Pallas, S. L. (2001). NMDA antagonists in the superior colliculus prevent
 634 developmental plasticity but not visual transmission or map compression. *Journal of*
 635 *Neurophysiology*, 86(3), 1179-1194. doi:10.1152/jn.2001.86.3.1179
- 636 Iwasato, T., et al. (1997). NMDA receptor-dependent refinement of somatotopic maps. *Neuron*
 637 *(Cambridge, Mass.)*, 19(6), 1201-1210. doi:10.1016/S0896-6273(00)80412-2
- 638 Jaubert-Miazza, L., et al. (2005). Structural and functional composition of the developing
 639 retinogeniculate pathway in the mouse. *Visual Neuroscience*, 22(5), 661-676.
 640 doi:10.1017/S0952523805225154
- 641 Johnson, K. O., & Triplett, J. W. (2021). Wiring subcortical image-forming centers: Topography,
 642 laminar targeting, and map alignment. *Current Topics in Developmental Biology*, 142, 283-
 643 317. doi:10.1016/bs.ctdb.2020.10.004
- 644 Kay, R. B., et al. (2018). Visual subcircuit-specific dysfunction and input-specific mispatterning
 645 in the superior colliculus of fragile X mice. *Journal of Neurodevelopmental Disorders*, 10(1),
 646 23. doi:10.1186/s11689-018-9241-1
- 647 Kesner, P., et al. (2020). Postsynaptic and presynaptic NMDARs have distinct roles in visual
 648 circuit development. *Cell Reports (Cambridge)*, 32(4), 107955.
 649 doi:10.1016/j.celrep.2020.107955
- 650 King, A. J., et al. (1996). The development of topographically-aligned maps of visual and
 651 auditory space in the superior colliculus. *Progress in Brain Research*, 112, 335-350.
 652 doi:10.1016/s0079-6123(08)63340-3
- 653 Massey, S. C., & Miller, R. F. (1990). N-methyl-D-aspartate receptors of ganglion cells in rabbit
 654 retina. *Journal of Neurophysiology*, 63(1), 16-30. doi:10.1152/jn.1990.63.1.16

- 655 McLaughlin, T., et al. (2003). Retinotopic map refinement requires spontaneous retinal waves
 656 during a brief critical period of development. *Neuron*, 40(6), 1147-1160. doi:10.1016/S0896-
 657 6273(03)00790-6
- 658 Meister, M., et al. (1991). Synchronous bursts of action potentials in ganglion cells of the
 659 developing mammalian retina. *Science*, 252(5008), 939-943. doi:10.1126/science.2035024
- 660 Mittman, S., et al. (1990). Concomitant activation of two types of glutamate receptor mediates
 661 excitation of salamander retinal ganglion cells. *The Journal of Physiology*, 428(1), 175-197.
 662 doi:10.1113/jphysiol.1990.sp018206
- 663 Mize, R. R., & Butler, G. D. (2000). The NMDAR1 subunit of the N-methyl-D-aspartate receptor
 664 is localized at postsynaptic sites opposite both retinal and cortical terminals in the cat
 665 superior colliculus. *Visual Neuroscience*, 17(1), 41-53. doi:10.1017/s0952523800171044
- 666 Muir-Robinson, G., et al. (2002). Retinogeniculate axons undergo eye-specific segregation in
 667 the absence of eye-specific layers. *The Journal of Neuroscience*, 22(13), 5259-5264.
 668 doi:10.1523/JNEUROSCI.22-13-05259.2002
- 669 Munz, M., et al. (2014). Rapid hebbian axonal remodeling mediated by visual stimulation.
 670 *Science*, 344(6186), 904-909. doi:10.1126/science.1251593
- 671 Nicoll, R. A., & Malenka, R. C. (1999). Expression mechanisms underlying NMDA receptor-
 672 dependent long-term potentiation. *Annals of the New York Academy of Sciences*, 868, 515-
 673 525. doi:10.1111/j.1749-6632.1999.tb11320.x
- 674 Paoletti, P., et al. (2013). NMDA receptor subunit diversity: Impact on receptor properties,
 675 synaptic plasticity and disease. *Nature Reviews. Neuroscience*, 14(6), 383-400.
 676 doi:10.1038/nrn3504

- 677 Pfeiffenberger, C., et al. (2005). Ephrin-as and neural activity are required for eye-specific
 678 patterning during retinogeniculate mapping. *Nature Neuroscience*, 8(8), 1022-1027.
 679 doi:10.1038/nn1508
- 680 Pfeiffenberger, C., et al. (2006). *Ephrin-as and patterned retinal activity act together in the*
 681 *development of topographic maps in the primary visual system*. Washington, D.C. : Society
 682 for Neuroscience. doi:10.1523/JNEUROSCI.3595-06.2006
- 683 Pittaluga, A., & Raiteri, M. (1990). Release-enhancing glycine-dependent presynaptic NMDA
 684 receptors exist on noradrenergic terminals of hippocampus. *European Journal of*
 685 *Pharmacology*, 191(2), 231-234. doi:10.1016/0014-2999(90)94153-O
- 686 Rajan, I., et al. (1999). NMDA receptor activity stabilizes presynaptic retinotectal axons and
 687 postsynaptic optic tectal cell dendrites in vivo. *Journal of Neurobiology*, 38(3), 357-368.
 688 doi:10.1002/(SICI)1097-4695(19990215)38:33.0.CO;2-#
- 689 Ruthazer, E. S., et al. (2003). Control of axon branch dynamics by correlated activity in vivo.
 690 *Science*, 301(5629), 66-70. doi:10.1126/science.1082545
- 691 Ruthazer, E. S., & Cline, H. T. (2004). Insights into activity-dependent map formation from the
 692 retinotectal system: A middle-of-the-brain perspective. *Journal of Neurobiology*, 59(1), 134-
 693 146. doi:10.1002/neu.10344
- 694 Schindelin, J., et al. (2012). Fiji: An open-source platform for biological-image analysis. *Nature*
 695 *Methods*, 9(7), 676-682. doi:10.1038/nmeth.2019
- 696 Schmittgen, T. D., & Livak, K. J. (2008). Analyzing real-time PCR data by the comparative C T
 697 method. *Nature Protocols*, 3(6), 1101-1108. doi:10.1038/nprot.2008.73

- 698 Shen, Y., et al. (2006). N-methyl-d-aspartate receptors in the retina. *Molecular Neurobiology*,
699 34(3), 163-179. doi:10.1385/MN:34:3:163
- 700 Simon, D. K., et al. (1992). N-methyl-D-aspartate receptor antagonists disrupt the formation of a
701 mammalian neural map. *Proceedings of the National Academy of Sciences of the United*
702 *States of America*, 89(22), 10593-10597. doi:10.1073/pnas.89.22.10593
- 703 Smetters, D. K., et al. (1994). An N-methyl- D-aspartate receptor antagonist does not prevent
704 eye-specific segregation in the ferret retinogeniculate pathway. *Brain Research*, 658(1),
705 168-178. doi:10.1016/S0006-8993(09)90023-3
- 706 Sweeney, N. T., et al. (2019). Expression of transcription factors divides retinal ganglion cells
707 into distinct classes. *Journal of Comparative Neurology (1911)*, 527(1), 225-235.
708 doi:10.1002/cne.24172
- 709 Triplett, J. W., et al. (2011). Competition is a driving force in topographic mapping. *Proceedings*
710 *of the National Academy of Sciences of the United States of America*, 108(47), 19060-
711 19065. doi:10.1073/pnas.1102834108
- 712 Tsien, J. Z., et al. (1996). The essential role of hippocampal CA1 NMDA Receptor–Dependent
713 synaptic plasticity in spatial memory. *Cell*, 87(7), 1327-1338. doi:10.1016/S0092-
714 8674(00)81827-9
- 715 Watanabe, M., et al. (1994). Differential distributions of the NMDA receptor channel subunit
716 mRNAs in the mouse retina. *Brain Research*, 634(2), 328-332. doi:10.1016/0006-
717 8993(94)91938-0
- 718 Wong, R. O. L., et al. (1993). Transient period of correlated bursting activity during development
719 of the mammalian retina. *Neuron*, 11(5), 923-938. doi:10.1016/0896-6273(93)90122-8

720 Xu, H., et al. (2015). Spatial pattern of spontaneous retinal waves instructs retinotopic map
721 refinement more than activity frequency. *Developmental Neurobiology*, 75(6), 621-640.
722 doi:10.1002/dneu.22288

723 Zhang, J., et al. (2016). (b). High-resolution quantitative immunogold analysis of membrane
724 receptors at retinal ribbon synapses. *Journal of Visualized Experiments*, (108), 53547.
725 doi:10.3791/53547

726 Zhang, R., et al. (2016). (a). Stereotyped initiation of retinal waves by bipolar cells via
727 presynaptic NMDA autoreceptors. *Nature Communications*, 7(1), 12650.
728 doi:10.1038/ncomms12650

729

730

731 **Figure Legends**

732 **Figure 1. Retina-specific knockout of GluN1 in Chrnb3-Cre;GluN1^{flox/flox} mice.** (A) Flat-
733 mounted retina of a Chrnb3-Cre;Rosa^{LacZ} reporter mouse line. (B) Section through the retina of
734 a P8 Chrnb3-Cre;Rosa^{TdTom} reporter mouse reveal cells labelled in the ganglion cell layer
735 (green). (C & D) Sections through the retina of P4 Ctl (C) and pre-cKO (D) mice labeled with
736 GluN1 antisense probe (arrowheads). *GCL*, ganglion cell layer; *IPL*, inner plexiform layer; *INL*,
737 inner nuclear layer; *OPL*, outer plexiform layer; *ONL*, outer nuclear layer (E & F) Sagittal
738 sections through the midbrain of P4 Ctl (E) and pre-cKO (F) mice labeled with GluN1 antisense
739 probe and higher magnification of GluN1 of the superficial and deep layers of the Ctl (E') and
740 pre-cKO (F') SCs. (G) Schematic of the GluN1 allele and approximate locations of the different
741 primer sets for qPCR and LoxP sites. (H & I) qPCR data for P0 micro-dissected retina (H) and
742 P0 SC (I) between Ctl and pre-cKO mice.

743
744 **Figure 2. Cytoarchitecture of retina unchanged in Chrnb3-Cre;GluN1^{flox/flox} mice.** (A-J)
745 Sections through the retinas of P4 Ctl (A-E) and pre-cKO (F-J) mice stained for RBPMS (A & F),
746 Brn3a (B & G), SatB2 (C & H), Beta3 (D & I), and calretinin (E & J). (K-O) Quantification of the
747 density of cells labeled with markers used in (A-J).

748
749 **Figure 3. Retinofugal topography is unaltered in Chrnb3-Cre;GluN1^{flox/flox} mice.** (A & B)
750 Whole-mount fluorescent images of the termination zones (TZs) of labeled RGCs observed in
751 the SC (dashed area) for Ctl (A) and pre-cKO (B) mice and coronal sections through the
752 corresponding TZs (A' & B'). *P*, posterior; *L*, lateral; *D*, dorsal (C) Quantification of the
753 termination zone indices (TZIs) in the SC. (D & E) Coronal sections through the dLGN of Ctl (D)
754 and pre-cKO (E) mice reveal the TZs of labeled RGCs. (F) Quantification of the termination
755 zone indices (TZIs) in the dLGN.

756

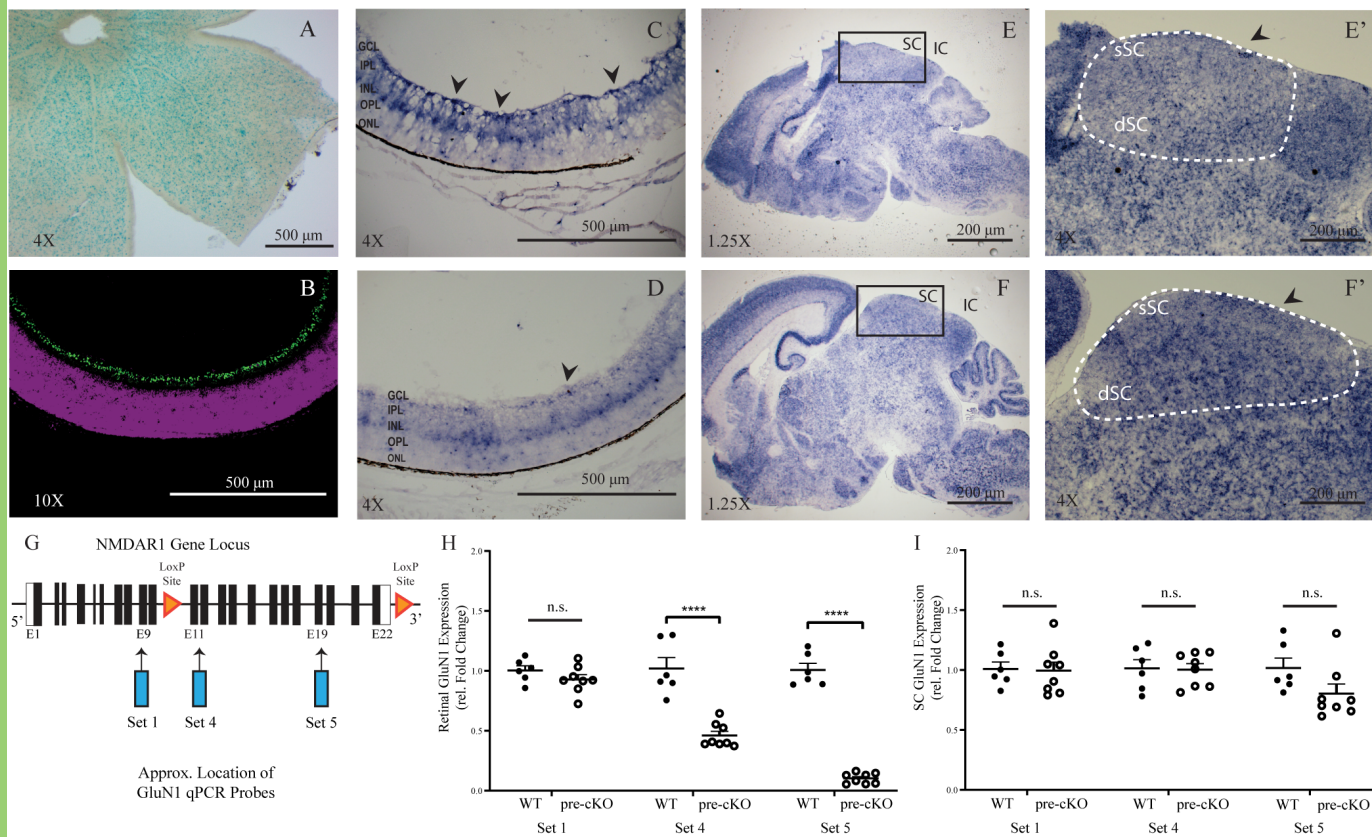
757 **Figure 4. Mature organization of eye-specific segregation in the dLGN is unaltered in**
758 **Chrn3-Cre;GluN1^{flox/flox} mice.** (A-F) Coronal sections through the dLGN of Ctl (A-C) and pre-
759 cKO (D-F) reveal the terminals of bulk labelled RGCs originating from the contralateral (A & D)
760 or ipsilateral (B & E) eye, as well as the degree of overlap (C & F). *D, dorsal; M, medial* (G)
761 Quantification of the amount of overlapping contralateral and ipsilateral inputs to the dLGN.

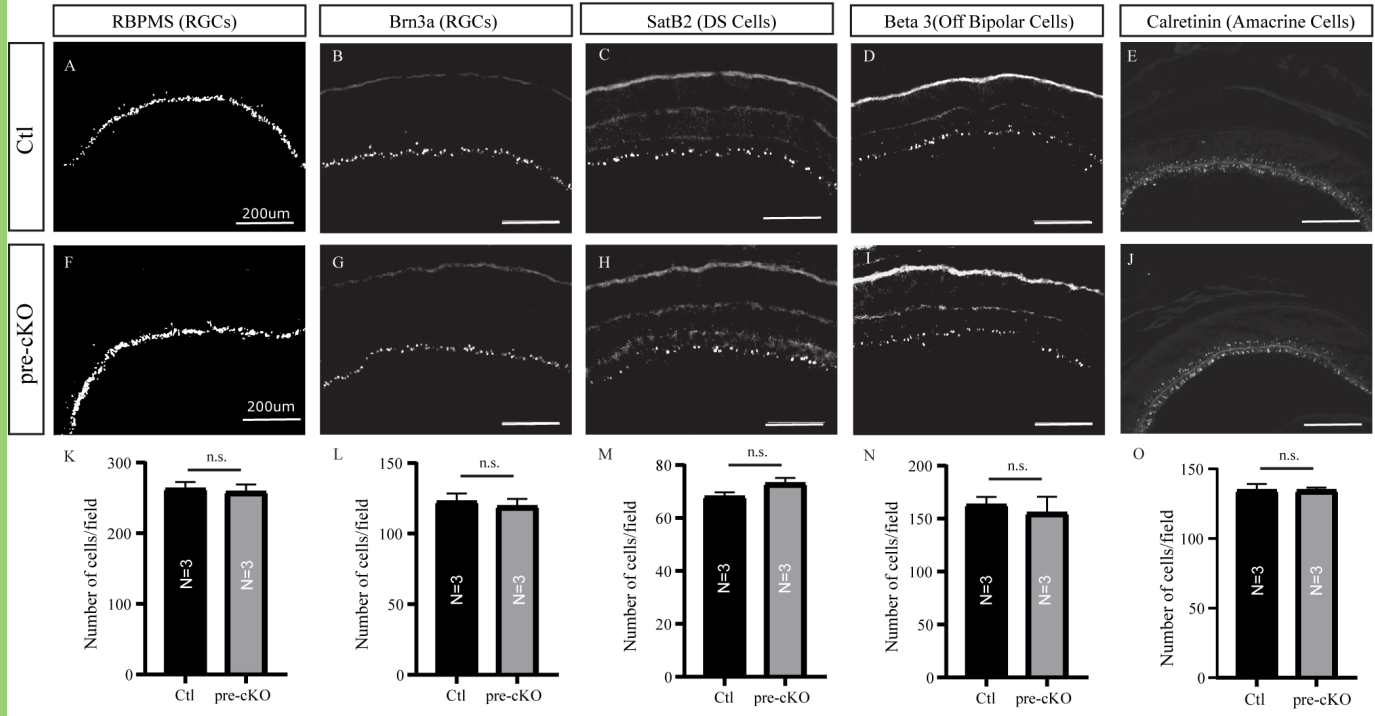
762
763 **Figure 5. Mature organization of eye-specific segregation in the SC is unaltered in**
764 **Chrn3-Cre;GluN1^{flox/flox} mice.** (A-F) Coronal sections through the SC of Ctl (A-C) and pre-
765 cKO (D-F) reveal the terminals of bulk labelled RGCs originating from the contralateral (A & D)
766 or ipsilateral (B & E) eye, as well as the degree of overlap (C & F). *D, dorsal; M, medial* (G)
767 Quantification of the amount of overlapping contralateral and ipsilateral inputs to the SC.

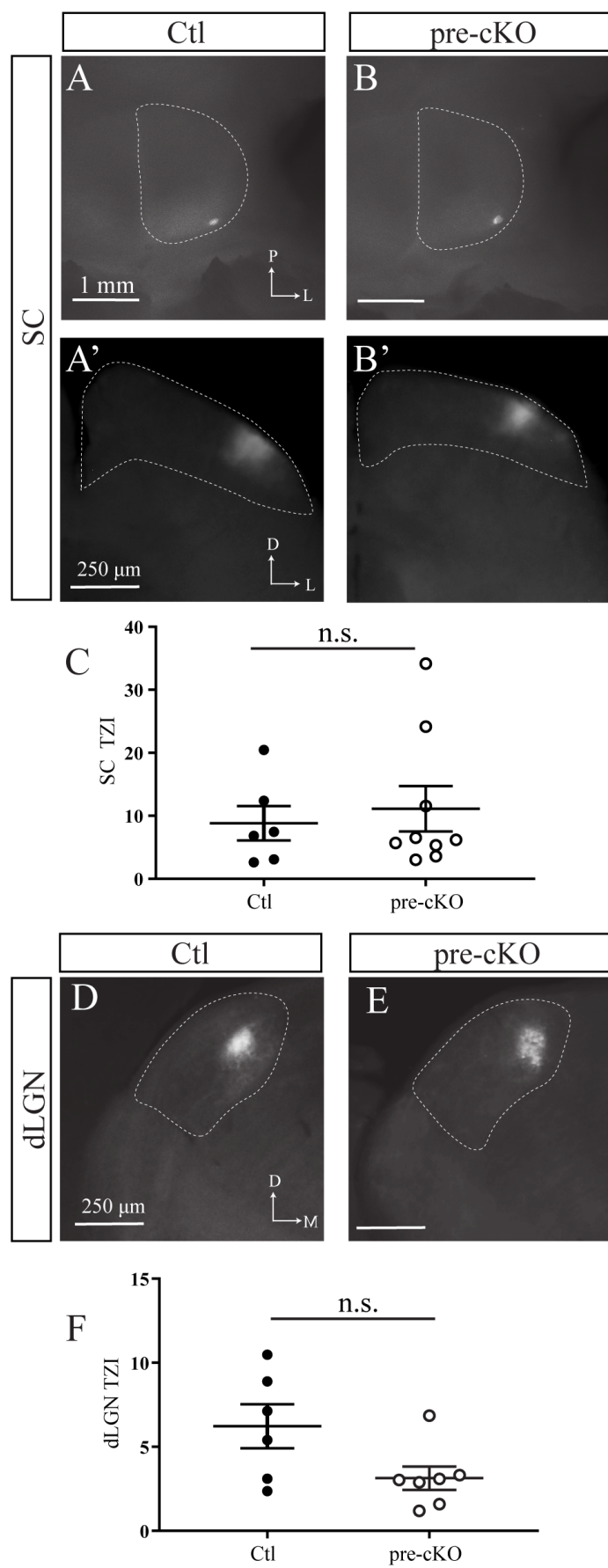
768
769 **Figure 6. Developmental trajectory of eye-specific segregation in the SC is unaltered in**
770 **Chrn3-Cre;GluN1^{flox/flox} mice.** (A-F) Coronal sections through the SC of Ctl (A-C) and pre-
771 cKO (D-F) reveal the terminals of bulk labelled RGCs originating from the contralateral (green)
772 and ipsilateral (magenta) eyes at postnatal day 4 (P4) (A & D), P8 (B & E), and P12 (C & F). *D,*
773 *dorsal; M, medial* (G) Quantification of the amount of overlapping contralateral and ipsilateral
774 inputs to the dLGN over the ipsilateral area at the indicated ages in Ctl and pre-cKO mice. (H)
775 Quantification of the amount of overlapping contralateral and ipsilateral inputs to the dLGN of Ctl
776 and pre-cKO mice at indicated ages, presented as the percent of the total dLGN area. (I)
777 Quantitative comparison of the ipsilateral patch length between Ctl and pre-cKO at indicated
778 ages, expressed as the percentage of the dLGN length covered by the ipsilateral patch along
779 the DM-VL axis.

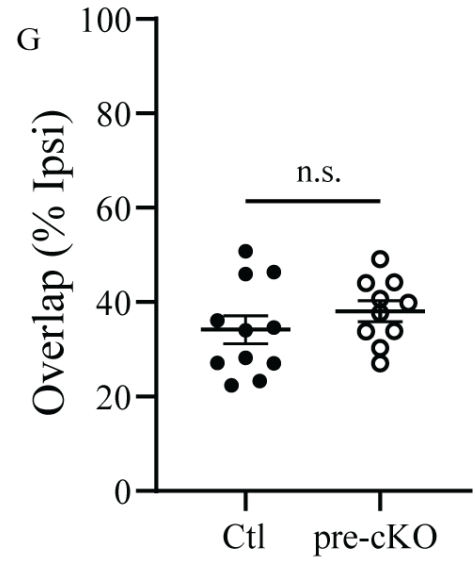
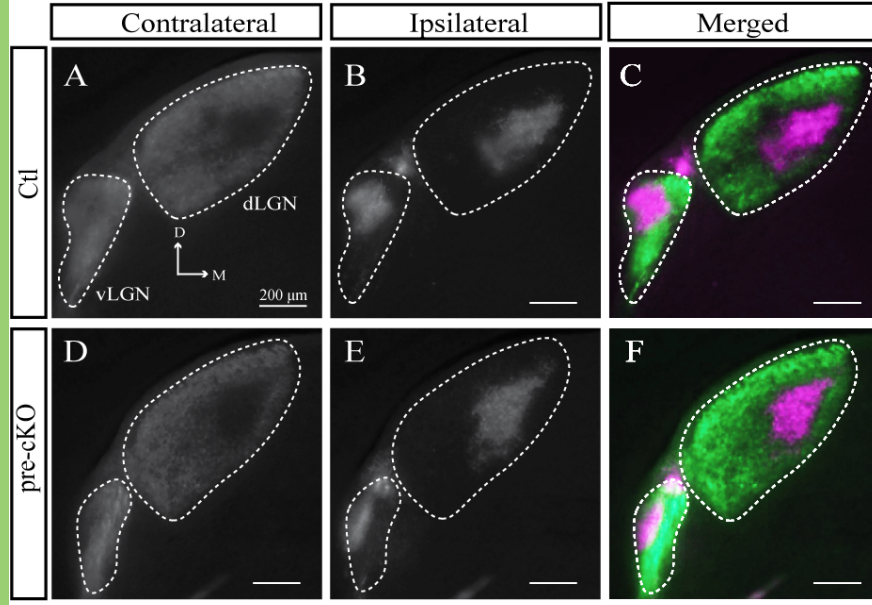
780
781 **Figure 7. NMDA elicited Ca²⁺ transients in the terminals of developing RGCs.** (A-D) Time
782 series fluorescent imaging of Ca²⁺ response in RGC terminals elicited in acute brain slices from

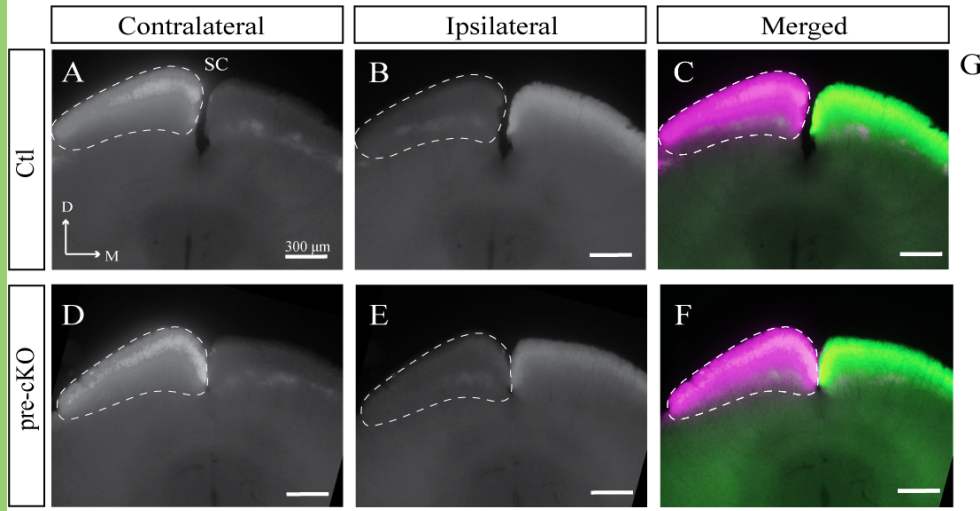
783 P6 Chrb3-Cre;GCaMP5::TdTom mice by focal application of NMDA in the SC in Mg^{2+} -free
784 aCSF (A), NMDA stimulation in the SC in aCSF (B), NMDA stimulation in the SC in Mg^{2+} -free
785 aCSF + MK-801 (C), and K^+ stimulation in the SC in aCSF (D) from a glass pipette (white
786 dashes in center panel). Graphs of change in fluorescence over time at four different regions of
787 interest (dashed colored circles) reveal the response elicited under each condition (right
788 panels). (E) Quantification of the peak $\Delta F/F$ (%) in the indicated conditions.











G

